Accepted Manuscript

The effective fracture strength and fracture toughness of solids with energy dissipation confined to localized strips

Xiaguang Zeng, Yujie Wei

PII: S0749-6419(18)30805-2

DOI: https://doi.org/10.1016/j.ijplas.2019.03.006

Reference: INTPLA 2503

To appear in: *International Journal of Plasticity*

Received Date: 7 December 2018

Revised Date: 16 March 2019

Accepted Date: 16 March 2019

Please cite this article as: Zeng, X., Wei, Y., The effective fracture strength and fracture toughness of solids with energy dissipation confined to localized strips, *International Journal of Plasticity*, https://doi.org/10.1016/j.ijplas.2019.03.006.

The effective fracture strength and fracture toughness of solids with energy dissipation confined to localized strips

Xiaguang Zeng [a], Yujie Wei [b,c*]

[a] School of Mechatronics Engineering, Foshan University, Guangdong 528000, China

[b] LNM, Institute of Mechanics, Chinese Academy of Sciences, Beijing 100190, China

[c] School of Engineering Sciences, University of Chinese Academy of Sciences, Beijing 100049, China

*Corresponding author: yujie_wei@lnm.imech.ac.cn

Abstract: Inelastic localized deformation in front of a crack tip dissipates energy and toughens the material. Such concentrated deformation could be resulted from plastic localization in solids, such as interfacial sliding in composites composing of heterogeneous layers, or by shear banding as seen in bulk metallic glasses (BMGs). The mechanisms of the localized deformation and the size of such events are crucial for the effective fracture properties of those particular solids. In this paper, we investigate the effective fracture strength and fracture toughness of solids where dissipation is dominantly contributed from plasticity in narrow strips by shear banding or interfacial sliding. We derive the analytical solutions in solids where energy dissipation occurs in co-planar elastic-perfectly plastic strips with strain softening, and also give approximate formulas of the effective strength and toughness for the solids with symmetric plastic strips. The toughening as a function of branching angle, thickness, yield stress, strength-softening ratio and local fracture toughness of the strips is determined quantitatively. The theory is also verified using finite-element (FE) simulations. These theoretical and finite element analysis supply a base for the design of strong and tough materials in which the plastic deformation is restricted within strips.

Keywords: Effective toughness; Fracture strength; Strain softening; Shear banding; Strip-yield model

1. Introduction

Inelastic deformation around a crack front contributes to energy dissipation in orders of magnitude higher than that of generating new surfaces (Erdogan, 2000; Irwin, 1957). Since this finding in the 1950s, it has been a great interest of the engineering community to explore the relationship between the fracture strength or the fracture toughness of ductile solids and their plastic deformation mechanisms (Barenblatt, 1962; Dugdale, 1960; Hutchinson, 1968; Pardoen et al., 2005; Rice and Rosengren, 1968; Rice and Sorensen, 1978; Tvergaard and Hutchinson, 1992; Wei and Hutchinson, 1997). It is generally recognized that the plasticity mechanisms and the size of such localized deforming zones are crucial for the fracture mechanical properties of a particular solid (Barthelat, 2014; Becher et al., 1988; Bohnert et al., 2016; Chen and Dai, 2016; Das et al., 2005; Gao et al., 1997; Kinloch et al., 1983; Zhou and Chen, 2016). Reliable theoretical analysis may help to identify crucial factors governing the fracture strength and toughness of such localized yielding materials, and enable us to further tune the microstructure of the materials for better performance in damage tolerance. That is particularly meaningful for some advanced materials where plastic deformation is not homogeneous due to the presence of structural heterogeneity.

Taking bulk metallic glasses (BMGs) as an example, their plasticity around a crack front is accommodated by shear bands whose width is on the order of several to tens of nanometers (Jiang et al., 2009; Jiang and Atzmon, 2006; Li et al., 2002) but can be as long as the sample dimensions. BMGs are originally isotropic homogeneous materials but become heterogeneous because of strength degradation in those strip regions. Such a mechanism resembles dislocation emission from a crack tip: while dislocations leave no lattice disturbance, the material in a shear band is relatively weaker than the intact counterpart. As illustrated in Fig. 1a, there are many shear bands in the palladium BMG, which shield an opening crack and promote its fracture toughness comparable to those of the toughest materials known (Demetriou et al., 2011). Such mechanism is broadly observed in high strength yet tough BMGs (Das et al., 2005; He et al., 2012; Hofmann

et al., 2008; Liu et al., 2007; Schroers and Johnson, 2004), as well as in amorphous polymers (Argon and Cohen, 1990; Friedrich, 1983; Spurr and Niegisch, 1962).

Crack-tip shielding resulted from localized deformation is not unique to BMGs or amorphous polymers. Nature has utilized such a design motif to make strong yet tough composites with stacking brittle minerals and highly deformable weak layers in between. As shown in Fig. 1b, nacre from mollusk shells exemplifies the mechanical design for the damage-tolerant material with high volume-fraction of brittle yet hard minerals and low volume-fraction of tough yet soft organic layers (Barthelat, 2014). The "mortar" layers are believed to provide the dominant energy dissipation during the fracture of the material. Such staggered structure is ubiquitously found in many bio-materials including bones (Gupta et al., 2005) and spider silks (Keten et al., 2010).

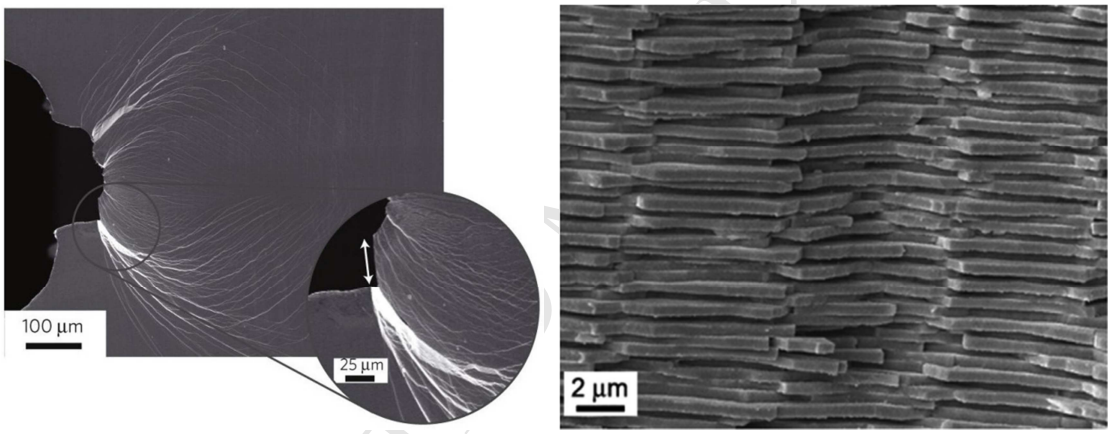

(a) (b)

Fig. 1. Two typical materials toughened by weak strips. (a) Shear banding in a palladium BMG which has a yield strength of 1490 MPa and a fracture toughness of 200 MPa $m^{0.5}$ (Demetriou et al., 2011). (b) A SEM image of nacre consisting of 95% of mineral bricks and 5% of protein and polysaccharide mortar (Barthelat, 2014).

For the aforementioned materials, the plastic "sliding" in preferential strips is the primary mechanism accounting for their fracture strengthening and toughening. Experiments on amorphous polymers (Argon and Cohen, 1990), on BMGs (Demetriou et al., 2011; He et al., 2012; Hofmann et al., 2008; Lei et al., 2015; Lewandowski et al., 2006; Liu et al., 2007; Schroers and Johnson, 2004), on nacre-like materials (Barthelat

and Espinosa, 2007; Naglieri et al., 2015; Niebel et al., 2016) and even on shales (Chandler et al., 2016; Na et al., 2017) all demonstrated that the shearing or softening introduced crack-tip shielding enhanced the damage-tolerance of these materials and gave rise to their fracture toughness enhancement. So far, how such energy dissipation mechanism via the weak strips quantitatively influence the effective fracture strength and toughness of such materials remains unclear.

The mechanical behavior of the layered solids heavily depends on the traction-separation constitutive models of the interfaces or heterogeneous layers, as illustrated by the elastic-plastic model (Anand et al., 2012; Su et al, 2004; McAuliffe and Waisman, 2015), the frictional cohesive model (Parrinello et al., 2009; Nguyen et al., 2017) and the stochastic model (Wei, 2014). Focusing on the fracture behavior of the layers, the crack strip-yield model (Dugdale, 1960; Barenblatt, 1962; Bilby et al., 1963; Burdekin and Stone, 1966) established an analytical relationship between the tensile loads and the length of the rigid plastic bands, which became a foundation to analyze the plastic banding influence on the fracture properties of the materials (Dowling and Townley, 1975; Budiansky and Hutchinson, 1978; Newman, 1984; Hillerborg, 1991; Yamada et al., 2011). Hutchinson and Suo (1992) presented a theoretical study on the cracking of a thin adhesive layer joining two identical bulk solids and suggested a local cracking morphology function to characterize the macroscopic toughness of such sandwich specimens. Their theory is applicable to brittle elastic media. Tvergaard and Hutchinson (1993, 1996) considered the crack propagation along the interface between a thin elastic-plastic adhesive layer and the elastic substrates, and numerically explored the influences of layer thickness, layer-substrate modulus mismatch and initial residual stress in the layer. Wei and Hutchinson (1997) numerically analyzed the crack opening growth accounting for the plastic dissipation in the layer-substrate solid. Estevez et al. (2000) investigated the competition between the shear yielding and crazing in the glassy polymer and the consequence on the material's fracture toughness. They found that the critical width of a craze appears to be a key feature in the polymer's toughness. Through cohesive models Wei et al. (2009) and

Shao et al. (2012) showed that fracture toughening by weak strips is dependent on the spacing of such zones as well as the mechanical properties of the strips. Hossain et al. (2014) numerically computed the effective toughness of heterogeneous media by the so-called surfing boundary condition and demonstrated that elastic heterogeneity can have a profound influence on fracture toughness, which not only toughens the material significantly but also leads toughness asymmetry.

In summary, regardless the tremendous progress about the contribution of the weak strips in crack front to fracture toughening, a concise and physically sound theory to predict both fracture strength and fracture toughness of such materials is not available so far. In this paper, we aim to connect the local mechanical properties of the strips to the effective fracture strength and toughness of the solids. We describe the problem in detail in Section 2, and give the analytical solutions to the effective fracture strength and toughness based on a modified strip-yield model in Section 3. Numerical validation to the theory is carried by using finite-element (FE) simulations, as seen in Section 4. We employ the theory to explore the dependence of fracture behavior on the properties of the strips in Section 5 and then discuss the difference between our model and the classic model in Section 6.

2. Problem description

We consider an infinite plate with a central slender throughout notch of length $2a$ and of root radius ρ. The plate is elastically isotropic with Young's modulus E and Poisson's ratio ν except the narrow strips in the notch front, whose plastic properties are distinct from those of the intact part, as shown in Fig. 2a. A far-field uniform tensile stress σ is applied in the direction perpendicular to a pre-existing notch. As we increase σ to a critical value σ_c, localized plastic deformation initiates from the notch tip in the form of shear bands or crazing strips with a thickness $t/2$ and a length s. Our focus is to quantify how the initiation and the extension of the strips influence the effective fracture strength and toughness of the plate. We assume plastic deformation is confined within the strips and the other parts of the plate deform elastically. For

simplicity, but without loss of physics, we consider a representative constitutive behavior in the strips, which exhibits linear elastic, strain softening and perfectly plasticity in response to separation. For comparison, we also consider a brittle response for the strips, as shown in Fig. 2b. We define σ_{y0}, ε_{y0}, and σ_{s0} in turn the yield stress, the yield strain, and the post-softening flow stress in the strip materials, and ε_{s0} is the strain when the softening initiates at σ_{s0}. Hence $E_s = \frac{\sigma_{y0} - \sigma_{s0}}{\varepsilon_{s0} - \varepsilon_{y0}}$ is the softening modulus. For the material in the strips, we assume von Mises yielding: it would yield and deform plastically when the von Mises stress σ_{e0} reaches the flow stress shown in Fig. 2b.

Let δ_n denote the displacement jump in the normal direction (separation) in the strips and δ_t that in the tangential direction. The critical values of the two displacements are δ_{nc} and δ_{tc}, beyond which the strips may fail. Following Tvergaard and Hutchinson (1993, 1996), we assume that such a strip would fracture when the work to separation (per unit area) of the strip equals to a critical value J_{Ic}, i.e., $J_{Ic} = \int_0^1 \sigma(\lambda)\mathrm{d}\lambda$ with $\lambda = \sqrt{(\delta_n/\delta_{nc})^2 + (\delta_t/\delta_{tc})^2}$. When brittle failure occurs, the energy release rate G_{Ic} is $\frac{\lambda\sigma_{e0}}{2}$, which coincides with the local fracture toughness J_{Ic} of the strip. Particularly in a purely normal separation situation, $G_{Ic} = \frac{t\sigma_{y0}^2}{2E}$, with $\sigma_{e0} = \sigma_{y0}$, $\lambda = t\varepsilon_0$ and $\varepsilon_0 = \frac{\sigma_{y0}}{E}$. For the special case of co-planar narrow strips (Fig. 2c), we may regard it as a localized necking problem of a thin plate weakened by a slender notch with circular root obeying the von Mises yield criterion, whose stress fields in the necking plastic zones ahead of the notch are similar to that of the necking problem of notched sheets solved by Hill (1952). Therefore, we hypothetically remove the plastic regions and assume that there is a uniform distributing of normal stress $\frac{2\sigma_{s0}}{\sqrt{3}}$ along the virtual upper and lower surfaces (red) and a normal stress $\frac{\sigma_{s0}}{\sqrt{3}}$ along the virtual notch side surfaces (green) according to the necking problem's solution, as shown in Fig. 2d.

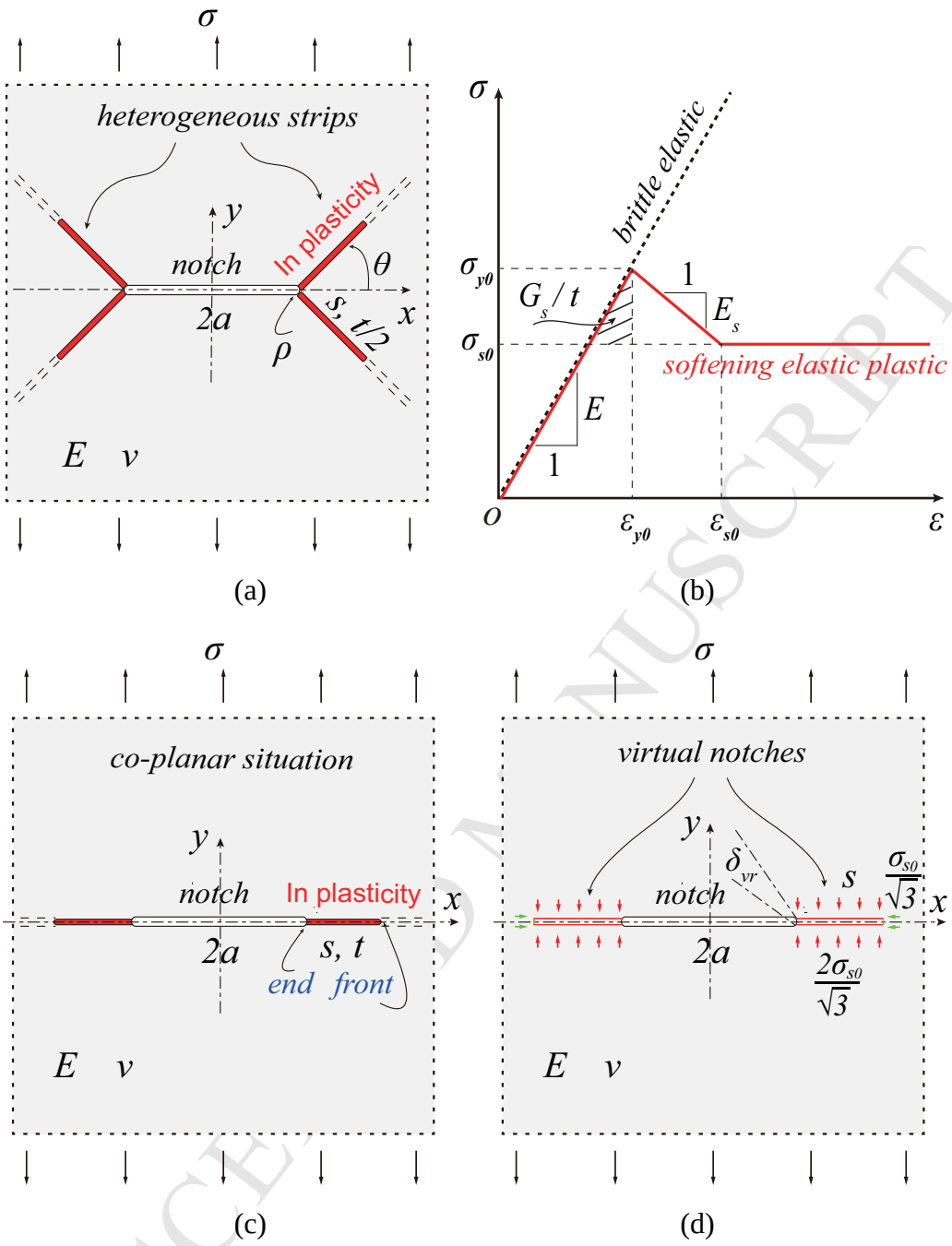

Fig. 2. Illustration of the heterogeneous weak strips around the fronts of the central notch. (a) A remote tensile plate with a central slender notch of length $2a$ and tip radius ρ. In front of the notch tip, there are symmetric weak plastic strips of length s, thickness $t/2$ and branching angle θ. Here $0 \le \theta \le \pi/2$, $\rho \ll a$, and $t \ll a$. (b) Representative stress-strain response of the strips, where σ_{y0} and σ_{s0} are respectively their yield stress and flow stress, ε_{y0} and ε_{s0} are the corresponding strains, and E_s denotes the softening modulus. (c) A remote tensile central notched plate with co-planar

strips, which corresponds to the special case of $\theta = 0$ in (a). (d) A modified strip-yield model for the co-planar strip case.

3. Theoretical derivation

Here we give the analytical solutions to the effective fracture strength and fracture toughness based on in turn the co-planar plastic strip model and the branching model shown in Fig 2. For clarity, we let σ_f, σ_f^b, σ_f^θ be the effective fracture strength of the specimens with co-planar plastic strips, with branching brittle interfaces and with branching plastic strips, respectively, and J_f, J_f^b, J_f^θ are their corresponding effective fracture toughness.

3.1. Co-planar softening plastic strip

We study the influence of strain softening in the elastic-plastic strips on the effective fracture toughness of the specimen shown in Fig. 2c where $\theta = 0$. Increasing in strip length s gives rise to the energy release resulted from the stress relaxation by strip front propagation. Meanwhile the original notch of length $2a$ may extend. Therefore, we need to determine the overall energy release rates both at the front and its end of one of the strips, as denoted in Fig. 2c. Following Dugdale (1960) and Barenblatt (1962), the plastically deformed field in the strips is of uniform stress. The plastic strips move forward and a new virtual notch of half length $a + s$ is created. According to Hill's solution to the necking localization problem of a tensile sheet weakened by circular notches obeying the von Mises yield criterion (Hill, 1952), we assume that a uniform normal stress $\frac{2\sigma_{s0}}{\sqrt{3}}$ is applied on the virtual surfaces, where σ_{s0} denotes the post-softening flow stress of the strips in uniaxial tension.

We now derive the energy release rate of the strip front with the elastic-perfectly plastic response with strain softening via the model shown in Fig. 2d. The stress

intensity factor of the corresponding crack strip-yield model given by Dugdale (Anderson, 2005) is

$$K_I = \sigma\sqrt{\pi(a+s)} - 4\sigma_{s0}\sqrt{\frac{a+s}{3\pi}}\operatorname{acos}(\frac{a}{a+s}). \quad (1)$$

For linear elastic solids, we have:

$$J_I = G_I = K_I^2/E. \quad (2)$$

According to Rice (1968), the energy release rate surrounding the virtual notch tip, J_{Iv}, is identical to the *J*-integral of the corresponding sharp crack with equivalent crack length as long as $(a+s) \gg t$. By substituting Eqn. (1) into Eqn. (2), we obtain the energy release rate of the strip front shown in Fig. 2c:

$$J_{Iv} = \frac{(a+s)\left[3\pi\sigma - 4\sqrt{3}\sigma_{s0}\operatorname{acos}\left(\frac{a}{a+s}\right)\right]^2}{9\pi E}. \quad (3)$$

To obtain the energy release rate of the strip end, we calculate the strip opening displacement (SOD) δ_{vr} at $x = a$, see Fig. 2d. As $(a+s) \gg \rho$ and $(a+s) \gg t$, we could use the SOD of the corresponding central crack model. Bilby et al. (1963) and Burdekin and Stone (1966) presented a solution to the SOD, i.e., $\frac{8a\sigma_{s0}}{\pi E}\ln\frac{a+s}{a}$, by assuming rigid plastic deformation in the strip, where $\sigma_{s0} = \sigma_{y0}$. The SOD δ_{vr} could be obtained by superimposing two elastic crack solutions δ_1 and δ_2. Here δ_1 is the solution to an infinite cracked plate subjected to uniform tensile stress $\frac{2\sigma_{s0}}{\sqrt{3}}$ along the plastic region, where $a < |x| < a+s$ and the Westergaard stress function is given as (Gdoutos, 2005)

$$Z_G = \frac{4\sigma_{s0}}{\sqrt{3}\pi}\left\{\frac{z}{\sqrt{z^2-(a+s)^2}}\operatorname{acos}\frac{a}{a+s} - \operatorname{acot}\left[\frac{a}{z}\sqrt{\frac{z^2-(a+s)^2}{(a+s)^2-a^2}}\right]\right\}, \quad (4)$$

with $z = x + iy$. Integrating the stress function in Eqn. (4) with respect to z, we have

$$Z_I = \frac{4\sigma_{s0}}{\sqrt{3}}\left\{\frac{\sqrt{z^2-(a+s)^2}}{\pi}\operatorname{acos}\frac{a}{a+s} - \frac{a}{\pi}\operatorname{atan}\left[\sqrt{\frac{z^2-(a+s)^2}{(a+s)^2-a^2}}\right] - \frac{z}{\pi}\operatorname{acot}\left[\frac{a}{z}\sqrt{\frac{z^2-(a+s)^2}{(a+s)^2-a^2}}\right]\right\}. \quad (5)$$

At $|x| = a$, the imaginary part of Z_I is

$$\operatorname{Im}(Z_I) = \frac{4\sigma_{s0}}{\sqrt{3}\pi}\left[\sqrt{s(2a+s)}\operatorname{acos}\frac{a}{a+s} + a\ln\frac{a}{a+s}\right]. \quad (6)$$

Then δ_1 at position $|x| = a$ for the plate subjected to uniformly distributed stress $\frac{2\sigma_{s0}}{\sqrt{3}}$ within the plastic zone $a < |x| < a + s$ is given as

$$\delta_1 = \frac{4}{E}\mathrm{Im}(Z_I) = \frac{16\sigma_{s0}}{\sqrt{3}\pi E}\left[\sqrt{s(2a+s)}\,\mathrm{acos}\frac{a}{a+s} + a\ln\frac{a}{a+s}\right]. \tag{7a}$$

The SOD of the central crack δ_2 at $|x| = a$ for the plate subject to a remote uniform stress σ is obtained by substituting $l = a + s$ and $|x| = a$ into the SOD formula $\delta_2 = \frac{4\sigma}{E}\sqrt{l^2 - x^2}$ (Tada et al., 2000). Hence we obtain

$$\delta_2 = \frac{4\sigma}{E}\sqrt{s(2a+s)}. \tag{7b}$$

Now δ_{vr} at the position $|x| = a$ for the infinite central notched plate subjected the remote tension σ and locally distributed stress $\frac{2\sigma_{s0}}{\sqrt{3}}$ in the plastic strip is obtained by combining Eqns. (7a) with (7b),

$$\delta_{vr} = \delta_2 - \delta_1 = \frac{4\sigma}{E}\sqrt{s(2a+s)} - \frac{16\sigma_{s0}}{\sqrt{3}\pi E}\left[\sqrt{s(2a+s)}\,\mathrm{acos}\frac{a}{a+s} + a\ln\frac{a}{a+s}\right]. \tag{8}$$

Within the case of rigid plasticity in the strip, there is $\frac{a}{a+s} = \cos\frac{\sqrt{3}\pi\sigma}{4\sigma_{y0}}$ with the distributed stress $\frac{2\sigma_{y0}}{\sqrt{3}}$ (Anderson, 2005). Equation. (8) is simplified to $\delta_{vr} = \frac{16a\sigma_{y0}}{\sqrt{3}\pi E}\ln\frac{a+s}{a}$. It is noted that here we have a different coefficient from the solution given by Bilby et al. (1963) and Burdekin and Stone (1966), as those authors might only took account of the uniaxial plastic flow with value σ_{y0}.

The energy release rate of the strip end should consist of the elastic toughness G_{Ic} and the plastic contribution $\frac{2\sigma_{s0}}{\sqrt{3}}\delta_{vr}$ (Shih, 1987; Anderson, 2005). With Eqn. (8), we obtain the energy release rate of the strip end ($|x| = a$) of the central notched plate shown in Fig. 2c as

$$J_{Ir} = G_{Ic} + \frac{8\sigma\sigma_{s0}\sqrt{s(2a+s)}}{\sqrt{3}E} - \frac{32\sigma_{s0}^2}{3\pi E}\left[\sqrt{s(2a+s)}\,\mathrm{acos}\frac{a}{a+s} + a\ln\frac{a}{a+s}\right]. \tag{9}$$

According to the energy release rate fracture criterion (Hussain et al., 1973; Nuismer, 1975), when a strip starts to fracture, the energy release rate at its end should be equal to the local fracture toughness of the strip. Therefore, we obtain an equation governing the fracture behavior of the plastic strip:

$$J_{Ir}|_{\sigma=\sigma_f} = G_{Ic} + \frac{8\sigma_f\sigma_{s0}\sqrt{s_f(2a+s_f)}}{\sqrt{3}E} - \frac{32\sigma_{s0}^2\left[\sqrt{s_f(2a+s_f)}\,\mathrm{acos}\frac{a}{a+s_f}+a\ln\frac{a}{a+s_f}\right]}{3\pi E} = J_{Ic}, \quad (10a)$$

where s_f is the strip length when σ reaches the critical state $\sigma = \sigma_f$ to initiate fracture in the notched specimen in tension.

With the degradation in the plastically deformed strip, the propagation of the strip front also dissipates a certain amount of energy per unit area (Eqn. 3), denoted as G_s. An equation governing the plastic propagation behavior of the strip is obtained when $s > 0$:

$$J_{Iv} = \frac{(a+s)\left[3\pi\sigma-4\sqrt{3}\sigma_{s0}\,\mathrm{acos}\left(\frac{a}{a+s}\right)\right]^2}{9\pi E} = G_s. \quad (10b)$$

When $s = s_f$ and $\sigma = \sigma_f$ in Eqn. (10b), we could obtain the length s_f of the softening plastic strip and the corresponding effective fracture strength σ_f when the strip starts to fracture at its end. The explicit solutions of s_f and σ_f from Eqns. (10a) and (10b) are not available. We resort to solve any one of the following equations numerically,

$$G_{Ic} + 8\sigma_{s0}\sqrt{\frac{s_f G_s(2a+s_f)}{3\pi E(a+s_f)}} - \frac{32a\sigma_{s0}^2}{3\pi E}\ln\frac{a}{a+s_f} = J_{Ic}, \quad (11a)$$

and

$$\frac{(a+s_f)\left[3\pi E(J_{Ic}-G_{Ic})+32a\sigma_{s0}^2\ln\frac{a}{a+s_f}\right]^2}{192\pi s_f(2a+s_f)E\sigma_{s0}^2} = G_s. \quad (11b)$$

Once s_f is available, σ_f can be written in terms of known parameters via

$$\sigma_f = \sqrt{\frac{EG_s}{\pi(a+s_f)}} + \frac{4\sigma_{s0}}{\sqrt{3}\pi}\mathrm{acos}\frac{a}{a+s_f}, \quad (12a)$$

or

$$\sigma_f = \frac{\sqrt{3}E(J_{Ic}-G_{Ic})}{8\sigma_{s0}\sqrt{s_f(2a+s_f)}} + \frac{4\sigma_{s0}}{\sqrt{3}\pi}\mathrm{acos}\frac{a}{a+s_f} + \frac{4a\sigma_{s0}}{\pi\sqrt{3s_f(2a+s_f)}}\ln\frac{a}{a+s_f}. \quad (12b)$$

Finally, the effective fracture toughness of the plate with the co-planar softening elastic-perfectly plastic strips shown in Fig. 2c is obtained via $J_f = \frac{\pi a\sigma_f^2}{E}$ (Anderson, 2005) and is given in the form of

$$J_f = \frac{aG_s}{a+s_f} + 8a\sigma_{s0}\text{acos}\frac{a}{a+s_f}\left[\sqrt{\frac{G_s}{3\pi(a+s_f)E}} + \frac{2\sigma_{s0}}{3\pi E}\text{acos}\frac{a}{a+s_f}\right], \tag{13a}$$

or

$$J_f = \frac{a\left\{3\pi E(J_{Ic}-G_{Ic})+32\sigma_{s0}^2\left[\sqrt{s_f(2a+s_f)}\text{acos}\frac{a}{a+s_f}+a\ln\frac{a}{a+s_f}\right]\right\}^2}{192\pi s_f\sigma_{s0}^2(2a+s_f)E}. \tag{13b}$$

Now we focus on the certain amount of energy dissipating per unit area during the propagation of the strip front, G_s, which should be a material property parameter analogous to the fracture toughness J_{Ic}. For simplicity, we assume that the corresponding energy release rate G_s at the front of the plastic strip is equal to $\frac{(\delta_{y0}-\delta'_{s0})(\sigma_{y0}-\sigma_{s0})}{2}$, where $\delta_{y0} = t\varepsilon_{y0} = \frac{t\sigma_{y0}}{E}$ and $\delta'_{s0} = \frac{t\sigma_{s0}}{E}$, as shown in Fig. 2b. Letting $\gamma = \frac{\sigma_{s0}}{\sigma_{y0}}$ define the strength-softening ratio, we rewrite $G_s = \frac{t\sigma_{y0}^2(1-\gamma)^2}{2E} = G_{Ic}(1-\gamma)^2$. Now Eqns. (11a), (12a) and (13a) may be rewritten as:

$$1 = \frac{t\sigma_{y0}^2}{2EJ_{Ic}} - \frac{32a\gamma^2\sigma_{y0}^2}{3\pi EJ_{Ic}}\ln\frac{a}{a+s_f} + \frac{8\gamma(1-\gamma)\sigma_{y0}^2}{EJ_{Ic}}\sqrt{\frac{ts_f(2a+s_f)}{6\pi(a+s_f)}}, \tag{14a}$$

with

$$\frac{\sigma_f}{\sigma_{y0}} = (1-\gamma)\sqrt{\frac{t}{2\pi(a+s_f)}} + \frac{4\gamma}{\sqrt{3}\pi}\text{acos}\frac{a}{a+s_f}, \tag{14b}$$

and

$$\frac{J_f}{a\sigma_{y0}} = \sigma_{y0}\left\{\frac{t(1-\gamma)^2}{2E(a+s_f)} + \text{acos}\frac{a}{a+s_f}\left[\frac{8(\gamma-\gamma^2)}{E}\sqrt{\frac{t}{6\pi(a+s_f)}} + \frac{16\gamma^2}{3\pi E}\text{acos}\frac{a}{a+s_f}\right]\right\}, \tag{14c}$$

respectively. For the elastic-perfectly plastic strip model, $G_s = 0$. We can then obtain the explicit formula of s_f and σ_f by solving Eqns. (10a) and (10b) with $\sigma_{s0} = \sigma_{y0}$. The two equations are given as

$$s_f = a\text{e}^{\frac{3\pi E(J_{Ic}-G_{Ic})}{32a\sigma_{y0}^2}}\left[1-\text{e}^{\frac{3\pi E(G_{Ic}-J_{Ic})}{32a\sigma_{y0}^2}}\right] = a\text{e}^{\frac{3\pi}{32}\left(\frac{EJ_{Ic}}{a\sigma_{y0}^2}-\frac{t}{2a}\right)}\left[1-\text{e}^{\frac{3\pi}{32}\left(\frac{t}{2a}-\frac{EJ_{Ic}}{a\sigma_{y0}^2}\right)}\right], \tag{15a}$$

and

$$\sigma_f = \frac{4\sigma_{y0}}{\sqrt{3}\pi}\text{acos}\left[\text{e}^{\frac{3\pi E(G_{Ic}-J_{Ic})}{32a\sigma_{y0}^2}}\right] = \frac{4\sigma_{y0}}{\sqrt{3}\pi}\text{acos}\left[\text{e}^{\frac{3\pi}{32}\left(\frac{t}{2a}-\frac{EJ_{Ic}}{a\sigma_{y0}^2}\right)}\right], \tag{15b}$$

respectively. The corresponding effective fracture toughness is

$$J_f = \frac{16a\sigma_{y0}^2}{3\pi E}\text{acos}^2\left[\text{e}^{\frac{3\pi E(G_{Ic}-J_{Ic})}{32a\sigma_{y0}^2}}\right] = \frac{16a\sigma_{y0}^2}{3\pi E}\text{acos}^2\left[\text{e}^{\frac{3\pi}{32}\left(\frac{t}{2a}-\frac{EJ_{Ic}}{a\sigma_{y0}^2}\right)}\right]. \tag{15c}$$

Notably, for the rigid plastic strip model, $G_s = G_{Ic} = 0$. We may further simplify Eqn. (15a-c) to

$$s_f = a(\mathrm{e}^{\frac{3\pi E J_{Ic}}{32a\sigma_{y0}^2}} - 1), \tag{16a}$$

$$\sigma_f = \frac{4\sigma_{y0}}{\sqrt{3}\pi}\mathrm{acos}(\mathrm{e}^{-\frac{3\pi E J_{Ic}}{32a\sigma_{y0}^2}}), \tag{16b}$$

and

$$J_f = \frac{16a\sigma_{y0}^2}{3\pi E}\mathrm{acos}^2(\mathrm{e}^{-\frac{3\pi E J_{Ic}}{32a\sigma_{y0}^2}}), \tag{16c}$$

respectively. The above equations describe the critical conditions when energy dissipation is confined within the plastic co-planar strips in front of the notch tips. Next we will consider more complicated scenarios when branching occurs in plastically deformed strips.

3.2. Branching softening plastic strip

In Fig. 2a, we showed branching strips forming a certain angle with respect to the original plane of the notch. We first consider the effective fracture toughness of the specimen with weak brittle elastic strips ahead of the notch tips. The strips are modeled as linear elastic brittle interfaces of zero thickness which have a fracture toughness J_{Ic}. We assume that the notch would only crack along the weak strips with a kinking angle θ. Based on these assumptions, we calculate the strain energy release rate of one notch tip in the kink direction. According to Nuismer (1975) and Zeng and Wei (2017), the strain energy release rate of the crack for potential deflection at an angle θ is given by

$$G_\theta = \begin{cases} \frac{K_{2\theta}^2}{E}, K_{1\theta} < 0 \\ \frac{K_{1\theta}^2 + K_{2\theta}^2}{E}, K_{1\theta} \geq 0 \end{cases}, \tag{17a}$$

with (Nuismer, 1975)

$$K_{1\theta} = \frac{1}{2}\cos\frac{\theta}{2}[K_I(1+\cos\theta) - 3K_{II}\sin\theta], \tag{17b}$$

$$K_{2\theta} = \frac{1}{2}\cos\frac{\theta}{2}[K_I\sin\theta + K_{II}(3\cos\theta - 1)], \tag{17c}$$

where K_I and K_{II} are the Mode I and Mode II stress intensity factors of the primary crack, respectively.

In the coordinate system given in Fig. 2a, $K_I = \sigma\sqrt{\pi a}$ and $K_{II} = 0$ (Anderson, 2005). Substituting K_I and K_{II} into Eqns. (17b) and (17c), then substituting them into Eqn. (17a), we obtain the strain energy release rate for the direction along angle θ as,

$$G_\theta = \frac{\pi a \sigma^2}{E}(\cos\frac{\theta}{2})^4. \tag{18}$$

According to Griffith's theory (1921), the fracture stress should be insensitive to the notch tip radius. Rice (1968) also showed the *J*-integral surrounding the notch tip is identical to the *J*-integral of the crack tip as long as $a \gg \rho$. Therefore, the central notch tip's strain energy release rate in the θ direction shown in Fig. 2a is G_θ in Eqn. (18). With the energy-based fracture criterion (Hussain et al., 1973; Nuismer, 1975), the notch begins to extend along the strip when G_θ equals to the fracture toughness of the interface, J_{Ic}. We hence obtain the fracture strength σ_f^b of the plate with brittle failure in the kinked strip within $0 \le \theta \le \pi/2$:

$$\sigma_f^b = \sqrt{\frac{EJ_{Ic}}{\pi a}}(\sec\frac{\theta}{2})^2. \tag{19}$$

The central notched plate with fracture strength σ_f^b has an effective fracture toughness $J_f^b = \frac{\pi a\left(\sigma_f^b\right)^2}{E}$ (Anderson, 2005). Taking Eqn. (19) into account, we obtain the effective fracture toughness of the central notched plate with weak branching brittle elastic interfaces,

$$J_f^b = J_{Ic}(\sec\frac{\theta}{2})^4. \tag{20}$$

It shows that both the local fracture toughness J_{Ic} of the strips and their branching angle determine the effective fracture toughness of the entire tensile specimen. Eqns. (19) and (20) are the products of two basic parts, i.e., local strength or toughness of the strips and a secant function of the deflection angle. By analogy, we utilize the effective fracture strength and toughness expressions for the co-planar plastic strips to construct approximate formulas of the effective fracture strength and toughness for the branching plastic strips in forms of

$$\sigma_f^{\theta} = \sigma_f(\sec\frac{\theta}{2})^{m/2}, \tag{21a}$$

and

$$J_f^{\theta} = J_f(\sec\frac{\theta}{2})^{m}, \tag{21b}$$

respectively, where m is a fitting parameter to be determined from FE simulations in next section, and σ_f and J_f are respectively the effective fracture strength and toughness of the aforementioned plate with the co-planar plastic strips.

4. Finite-element calculations

In the previous section, we have presented several analytical solutions to the effective fracture strength and toughness for the central notched specimen with co-planar plastic strips or branching brittle strips in nature. Here we perform FE calculations to verify these analytical results.

4.1. The finite-element model

For structural symmetry, we consider one fourth of the notched plate shown in Fig. 3. The length and width of the plate are about 25 times of the length of the notch and the strip. An isotropic elastic-plastic plane stress constitutive model is adopted for the material in the strip while the rest of the plate deforms elastically. Yielding in the strip follows the von Mises criterion and the plastic flow follows the stress-strain behavior with strain softening shown in Fig. 2b. The plane stress elements including CPS4 and CPS3 in ABAQUS (Simulia, 2011) are used. Mesh size sensitivity is carried out. The mesh size about one-tenth of the strip thickness in the strip and around the notch tip is sufficient to guarantee the convergence of the simulations. During the tensile deformation, we calculate the *J*-integral of the real notch tip in the strip direction. For a

given J_{Ic} of the strip, if the *J*-integral equals to it, we select the length of the plastically deforming strip and the corresponding tensile stress as the critical strip length s_f and the fracture strength σ_f of the specimen, respectively.

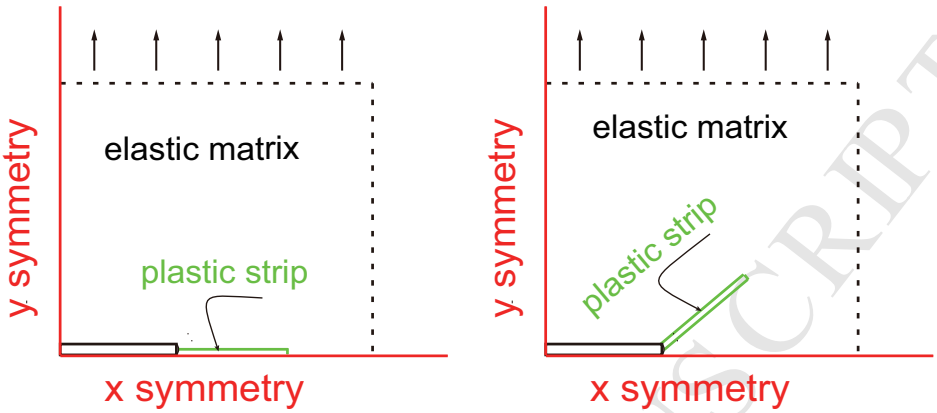

(a) co-planar case (b) branching case

Fig. 3. Finite-element models for the plate with a central notch and co-planar heterogeneous strips (a) or branching strips (b) ahead the notch tip. One quarter of the sample is used by accounting for the symmetry of the problem.

4.2. Deformation in the strip front

We present representative stress and strain fields around the notch front in a specimen with co-planar softening elastic-perfectly plastic strips in Fig. 4. The specimen is subject to a far-field tensile stress σ. The following dimensions and material parameters are used in the simulations, with $a = 5\text{mm}$, $t = 0.036a$, $E = 100\text{GPa}$, $\nu = 0.3$, $E_s = E/4 = 25\text{GPa}$, $\sigma_{y0} = 400\text{MPa}$, $\sigma_{s0} = 240\text{MPa}$, and $J_{Ic} = 4.8\text{kN/m}$. We show in Fig. 4a an elastically deformed strip at $\sigma = 36.0\text{MPa}$. When σ increases, the strip yields and propagates, and a stress field similar to a crack-tip stress field emerges around the strip front, as shown in Fig. 4b and Fig. 4c. When $\sigma = 117.4\text{MPa}$, the length of the plastically deforming strip reaches $0.17a$ (see

Fig. 4b) and the *J*-integral of the notch tip is equal to 2.4kN/m; when $\sigma = 158.9\text{MPa}$, the length of the plastically deforming strip is about $0.44a$ and the *J*-integral of the notch tip equals to 4.8kN/m, the same as the fracture toughness of the strip. Therefore, the fracture strength σ_f of the specimen is 158.9MPa, and the corresponding maximum length s_f of the plastic strip is $0.44a$. In Fig. 4d and Fig. 4e we further show the fields of σ_{yy} and ε_{yy} at this critical point when the plastic strip starts to fracture. The result suggests that our assumption of uniformly distributed stress on the strip surfaces is reasonable.

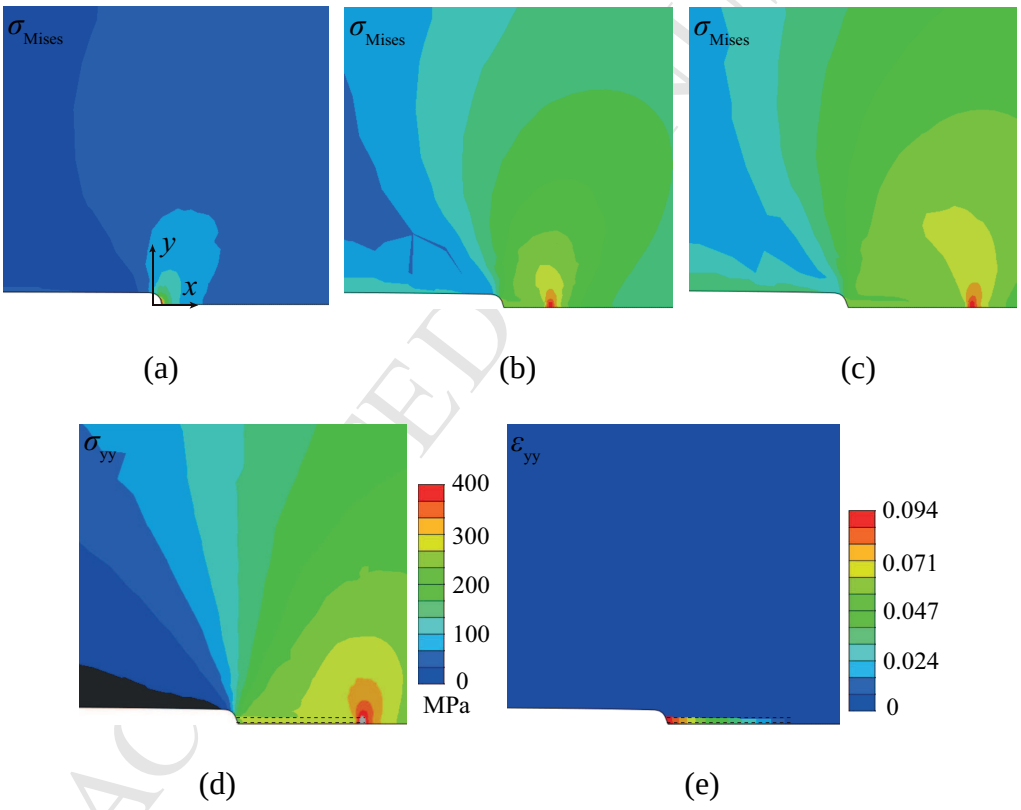

Fig. 4. Contour plots around the notch tip and the co-planar softening elastic-perfectly plastic strip during the tension process of the central notched plate, where the legend for stress is the same for (a)-(d). (a) Von Mises stress field when the strip is totally in elastic deformation. (b) Von Mises stress field when a part of the strip is in plastic deformation. (c) Von Mises stress field when the strip in plastic deformation starts to fracture. (d) The

stress σ_{yy} and (e) the strain ε_{yy} corresponding to the fracture moment shown in (c), where the plastically deforming zone is highlighted by the dashed lines.

We show in Fig. 5 the stress evolution of the branching strip with strain softening during the tension of the plate, where the related parameters are as follows: $a = 5\text{mm}$, $t = 0.036a$, $\theta = 45°$, $E = 100\text{GPa}$, $\nu = 0.3$, $E_s = E/4$, $\sigma_{y0} = 400\text{MPa}$, $\sigma_{s0} = 240\text{MPa}$, and $J_{Ic} = 4.8\text{kN/m}$. When $\sigma = 44.0\text{MPa}$, the strip begins to deform plastically in the matrix, as shown in Fig. 5a; When $\sigma = 126.7\text{MPa}$, about $0.25a$ length of the strip is in plastic deformation, as shown in Fig. 5b; and at σ=172.5MPa, the length of the plastically deforming strip is about $0.89a$, as shown in Fig. 5c. At this moment, the *J*-integral of the notch tip along the branching direction is equal to the strip's fracture toughness 4.8kN/m, so the fracture strength of the specimen is 172.5MPa and the corresponding critical length of the strip is $0.89a$. Compared with the co-planar strip case, the assumption on uniform stress distribution within the strip is no longer valid, as shown in Figs. 5d~f, which brings a great difficulty to derive analytical solutions to the effective fracture toughness of the plate with symmetric branching plastic strips.

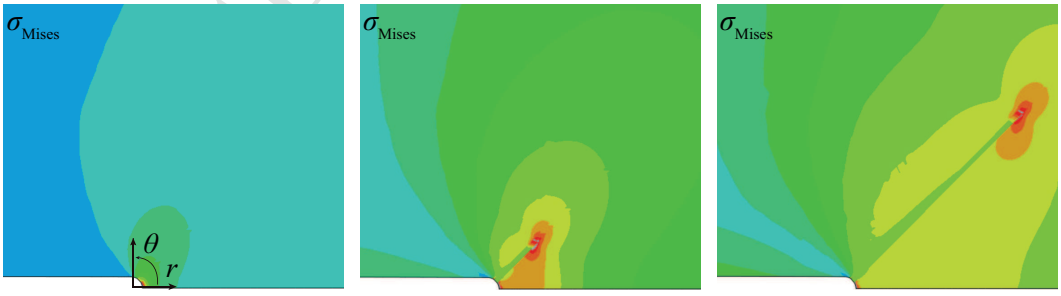

(a) (b) (c)

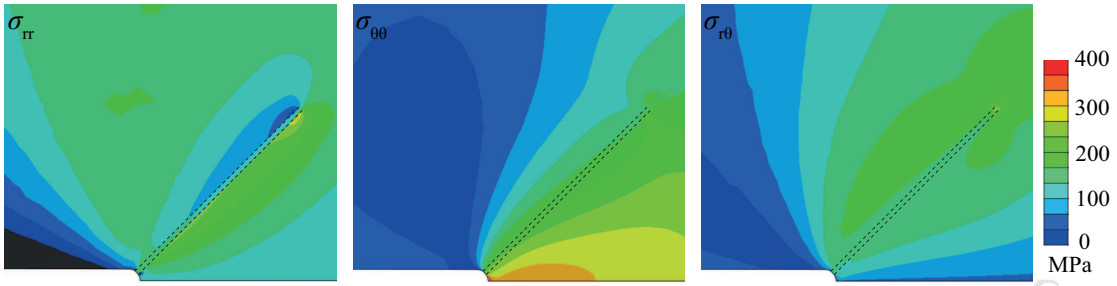

(d) (e) (f)

Fig. 5. Contour plots around the notch tip and the branching softening elastic-perfectly plastic strip during the tension process of the central notched plate. (a) Von Mises stress field when the strip begins to deform plastically. (b) Von Mises stress filed when a part of the strip is in plastic deformation. (c) Von Mises stress field when the strip in plastic deformation starts to fracture. (d) Radial stress, (e) hoop stress and (f) shear stress fields in the cylindrical coordinate corresponding to the fracture moment shown in (c), where the plastically deforming zone is highlighted by the dashed lines.

4.3. Numerical verification

Now we compare the FE results and our theoretical predictions for the central notched plate with the co-planar plastically deforming strips. In Fig. 6, we verify the two types of results showing the influence of the local fracture toughness J_{Ic} of the strips on the plastically deforming length of the strips and on the fracture strength of the specimen. For strength-softening ratio $\gamma = 1.0$, 0.8 and 0.6, we see that the plastic strip length and the specimen fracture strength are both increasing with an increasing normalized fracture toughness $\frac{J_{Ic}}{a\sigma_{y0}}$ of the plastic strips. Meanwhile we see good agreements

between the FE results and the corresponding theoretical predictions.

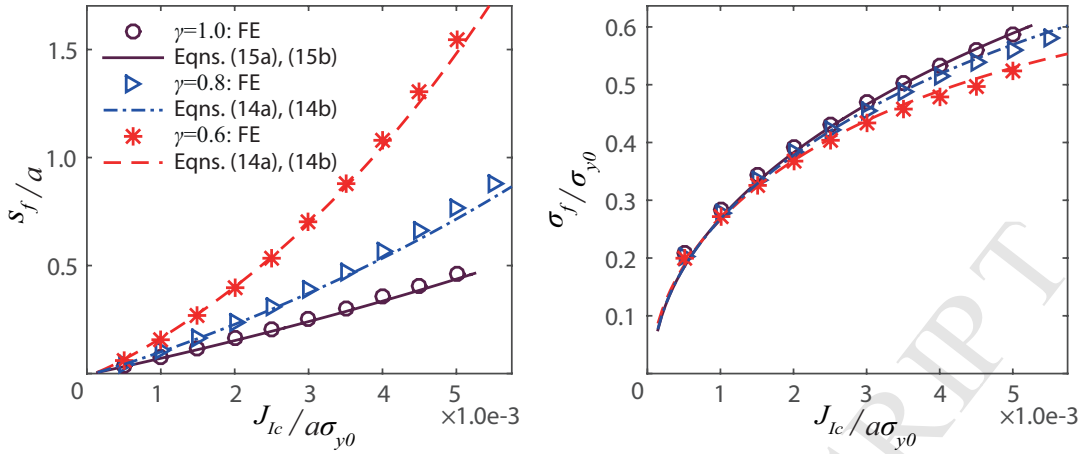

(a) (b)

Fig. 6. Comparison between the FE results and our theoretical predictions, which verifies the influence of the fracture toughness J_{Ic} of the weak plastic strips. (a) Normalized length of the co-planar plastically deforming strips as a function of normalized fracture toughness $\frac{J_{Ic}}{a\sigma_{y0}}$ with different values of the softening ratio γ, where the following parameters are used: $a = 5\text{mm}$, $t = 0.036a$, $E = 100\text{GPa}$, $\sigma_{y0} = 400\text{MPa}$, $J_{Ic} = 0.2\sim11.0\text{kN/m}$, $E_s = 2E$, E for $\gamma = 0.8,\ 0.6$ respectively. (b) The corresponding normalized fracture strength of the specimens.

We verify the influence of the strength-softening ratio γ of the strips on the plastically deforming length of the strips and on the fracture strength of the specimen in Fig. 7. For different softening modulus, $E_s = E/2,\ E/8$ for the plastic strips, we consider two different local fracture toughness values, $J_{Ic} = 5\text{kN/m}$ and 3kN/m. From the FE result sets for the four combinations, we see that with the decreasing softening ratio, the plastic strip length in the specimen increases progressively, but the corresponding fracture strength decreases progressively. The FE result sets for the two values of the softening modulus E_s show difference, especially in the critical length, which demonstrates that the influence of the softening ratio on the strip length and the effective strength depends on the softening modulus as well. However, our theoretical analysis does not take this into account and we see distinction between the FE and theoretical results. Fortunately, the effective strength has a much weaker dependence on

E_s, as shown in Fig. 7b. We also see good matches between the FE results and the theoretical predictions when $E_s = E/2$. In other words, if the softening modulus falls in a proper range, our theoretical solutions show reasonable predictability.

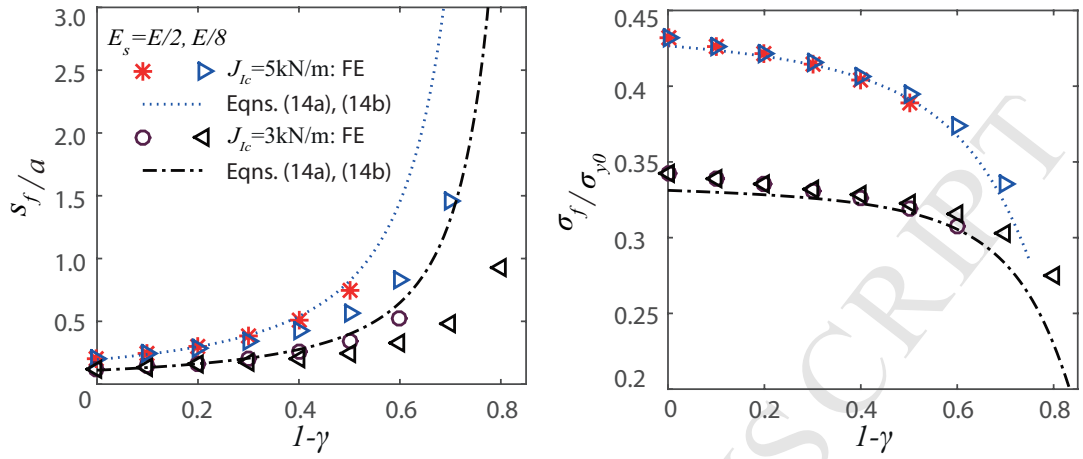

(a) (b)

Fig. 7. Comparison between the FE results and our theoretical predictions, which verifies the influence of the strength-softening ratio γ of the weak plastic strips. (a) Normalized length of the co-planar plastically deforming strips as a function of $1-\gamma$ with different values of softening modulus E_s and local fracture toughness J_{Ic}, where the following parameters are used: $a = 5\text{mm}$, $t = 0.036a$, $E = 100\text{GPa}$, $\sigma_{y0} = 400\text{MPa}$. (b) The corresponding normalized fracture strength of the specimens.

We further examine the influence of the softening modulus E_s of the strips on the plastically deformed length of the strips and on the fracture strength of the specimen, as shown in Fig. 8. In each case with softening ratio $\gamma = 0.8$ or 0.6, we consider two different local fracture toughness values, $J_{Ic} = 5\text{kN/m}$ and 3kN/m. The FE result sets of the four combinations imply that an increasing softening modulus increases the plastically deforming length of the strips, but decreases the fracture strength of the specimen. However, when $E_s > E/2$, the softening modulus has nearly no influence on the length and the strength. As shown in Fig. 8, although our theoretical derivation neglects the softening modulus effect, i.e., we assume that the energy release rate G_s at the plastic strip front is equal to $\frac{t\sigma_{y0}^2(1-\gamma)^2}{2E}$, we see good matches between the FE results and the theoretical predictions when $E_s > E/2$. In sum, all the agreements between the

FE results and the theoretical predictions shown in Figs. 6, 7 and 8 indicate that our assumption on G_s and the other simplifications seem to be reasonable approximations as long as $E_s > E/2$. Therefore, we could further use our analytical solutions Eqns. (14), (15) and (16) to explore the influence of the strips on the effective fracture toughness of the heterogeneous specimens.

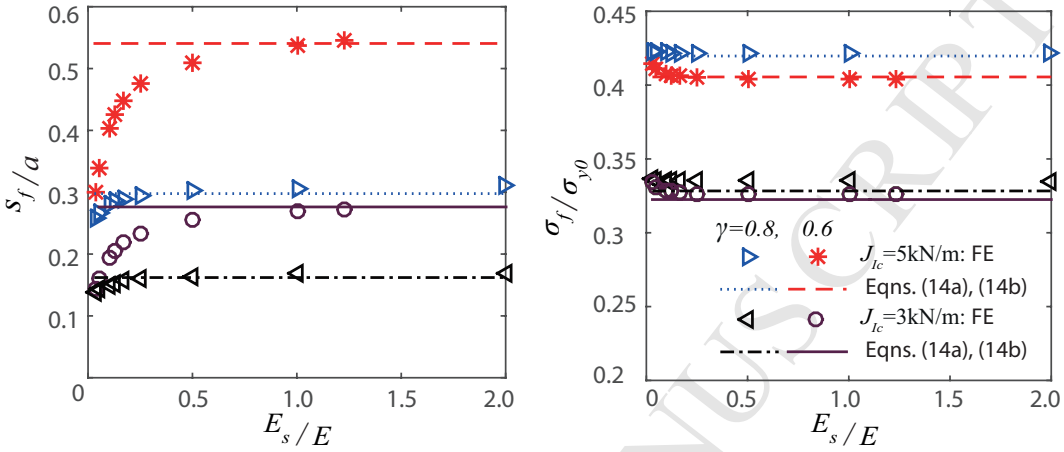

(a) (b)

Fig. 8. Comparison between the FE results and our theoretical predictions, which verifies the influence of the softening modulus E_s of the weak plastic strips. (a) Normalized length of the co-planar plastically deforming strips as a function of normalized softening modulus E_s/E with different values of the softening ratio γ and local fracture toughness J_{Ic}, where the following parameters are used: $a = 5\text{mm}$, $t = 0.036a$, $E = 100\text{GPa}$, $\sigma_{y0} = 400\text{MPa}$. (b) The corresponding normalized fracture strength of the specimens.

We have constructed two approximate formulas for the effective fracture strength and toughness of the notched plate with branching softening plastic strips, i.e., Eqns. (21a) and (21b). The two equations have an unknown parameter m. We determine $m = 2.6$ by fitting the FE results for the effective strength and toughness respectively, as shown in Fig. 9a and Fig. 9b. Here two different local fracture toughness values are considered, and we see that both scenarios have a reasonable agreement between the FE results and the fitting formulas.

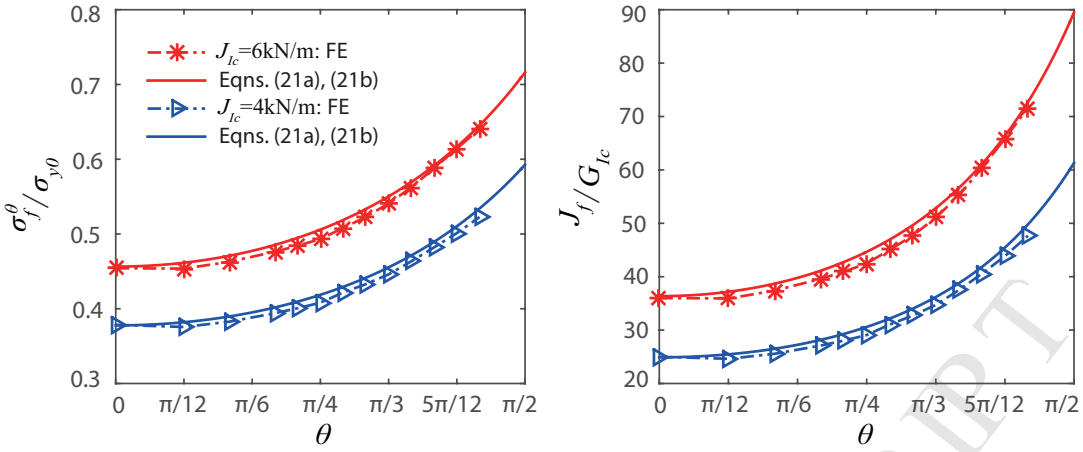

(a) (b)

Fig. 9. Determination of the value of m in Eqn. (21) by fitting the FE results, where (a) and (b) show the fitting results of the effective fracture strength Eqn. (21a) and the effective fracture toughness Eqn. (21b) respectively both with $m = 2.6$, where the following parameters are used: $a = 5\text{mm}$, $t = 0.036a$, $E = 100\text{GPa}$, $E_s = E/2$, $\sigma_{y0} = 400\text{MPa}$ and $\gamma = 0.8$.

5. Effective fracture toughness

For the plate with the co-planar softening elastic-perfectly plastic strips, Eqns. (14a) and (14c) indicate that the strip thickness t, yield stress σ_{y0}, strength-softening ratio γ and local fracture toughness J_{Ic} all have influences on the effective fracture toughness of the plate. According to the dimensional analysis theory (Anderson, 2005), we further define the dimensionless strip thickness $\frac{t}{a}$, yield stress $\frac{\sigma_{y0}}{E}$ and local toughness $\frac{J_{Ic}}{aE}$, where the notch length a and Young's modulus E are selected as the primary quantities. For the plate with the branching strips, Eqns. (20) and (21b) show that the branching angle θ also has an important influence on the effective fracture toughness of the specimen. Here we explore the influence of all these factors of the heterogeneous strips on the effective fracture toughness of the plate in detail.

5.1. The geometric parameters of strips

For the brittle branching strips, Eqn. (20) indicates that the branching angle increases the effective fracture toughness J_f^b in proportional to $(\sec\frac{\theta}{2})^4$. There is a maximum amplification factor "4" at $\theta = \pi/2$ for the effective toughness. For the plastically branching strips, Eqn. (21b) suggests that the branching angle increases the effective fracture toughness by approximately following the relationship of $(\sec\frac{\theta}{2})^{2.6}$. We see that the plate with branching strips always has a greater effective toughness than that with co-planar strips because both $(\sec\frac{\theta}{2})^4$ and $(\sec\frac{\theta}{2})^{2.6}$ are greater than 1 when $0 < \theta \leq \pi/2$. Meanwhile, it is seen that the brittle branching strips toughen the central notched plate in more drastic than the plastic branching strips do, as shown in Fig. 10a.

In addition, we examine the influence of the plastic strip thickness on the effective fracture toughness of the heterogeneous plate via Eqns. (14a) and (14c) with different strength-softening ratio γ, dimensionless yield stress $\frac{\sigma_{y0}}{E}$ and local toughness $\frac{J_{Ic}}{aE}$, as shown in Fig. 10b. We see that the effective fracture toughness of the plate has an almost linear dependence on the thickness of the co-planar plastic strips. Decreasing the softening ratio in turn from 1.0 to 0.6, to 0.4 and to 0.3, the strip thickness initially decreases the effective toughness and later increases it, and the critical softening ratio for the tendency transition is about 0.4 (see the blue horizontal dotted line) for the case with $a = 5\text{mm}$, $E = 100\text{GPa}$, $\sigma_{y0} = 400\text{MPa}$ and $J_{Ic} = 6\text{kN/m}$. The horizontality of the critical transition case suggests that the strip thickness has no influence on the

effective toughness. Actually, the critical transition state also depends on the dimensionless yield stress $\frac{\sigma_{y0}}{E}$ and local toughness $\frac{J_{Ic}}{aE}$. As $\frac{\sigma_{y0}}{E}$ decreases from 4e-3 to 2e-3 or as $\frac{J_{Ic}}{aE}$ increases from 1.2e-5 to 4e-5, we obtain two transition states from the basic case, as illustrated by the other two horizontal lines with circles or stars. The thickness influence may explain why there is a complex size effect of the notch tips in many BMGs' fracture experiments (Lowhaphandu and Lewandowski, 1998; Schroers and Johnson, 2004; Lewandowski et al., 2006).

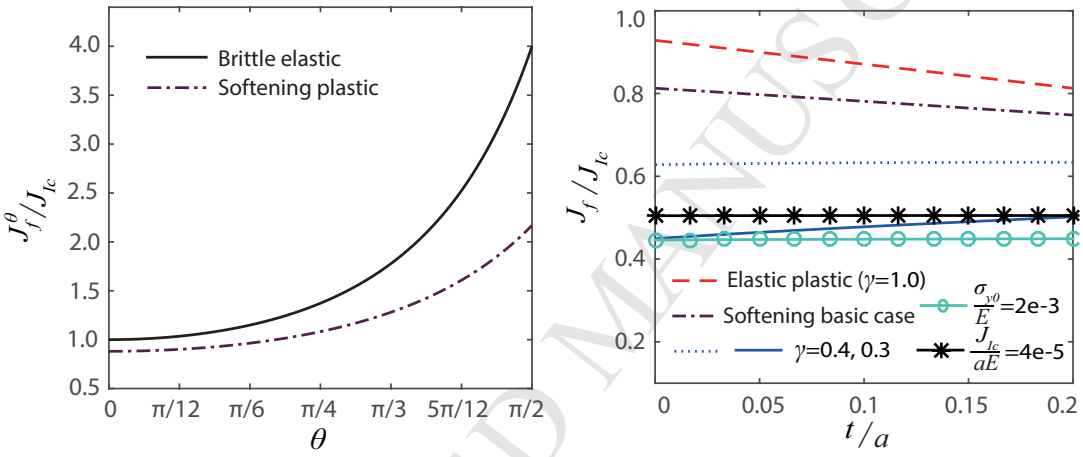

(a) (b)

Fig. 10. Influence of the strip geometric parameters on the normalized effective fracture toughness of the tensile central notched plate. (a) Influence of the strip branching angle, where the following parameters are used: $a = 5\text{mm}$, $t = 0.036a$, $E = 100\text{GPa}$, $\sigma_{y0} = 400\text{MPa}$, $\gamma = 0.8$, $J_{Ic} = 6\text{kN/m}$. (b) Influence of the strip thickness, where the softening basic case is plotted using Eqns. (14a) and (14c) with $a = 5\text{mm}$, $E = 100\text{GPa}$, $\sigma_{y0} = 400\text{MPa}$, $\gamma = 0.6$ and $J_{Ic} = 6\text{kN/m}$, and the other five cases are calculated by changing one parameter of the basic case as denoted in the figure.

5.2. Plastic property of strips

We reveal in Eqns. (14a), (14c), (15c) and (16c) that the plastic properties of the strips, such as the yield stress, have complex influences on the effective fracture toughness of the plate with the heterogeneous strips. We show the influence of the dimensionless yield stress and strength-softening ratio on the effective fracture toughness in Fig. 11a and Fig. 11b, respectively. The yield stress of the rigid plastic strips increases the effective toughness, while the yield stress of the elastic-plastic strips with softening initially increases the effective toughness and then decreases the effective toughness. For the latter case, there is an optimal yield stress for toughness. The value is sensitive to the softening ratio, dimensionless strip thickness and local toughness, as explored in Fig. 11a.

The influence of the strength-softening ratio γ is seen in Fig. 11b. Smaller softening ratio could often lead to lower effective fracture toughness. At a greater dimensionless thickness, such as 0.09, or at a higher dimensionless yield stress, such as 0.016, or at a smaller dimensionless local toughness, such as 6e-6, decreasing γ could initially increase the effective toughness and then decrease the effective toughness. The transitional region is sensitive to the dimensionless thickness, yield stress, and local toughness.

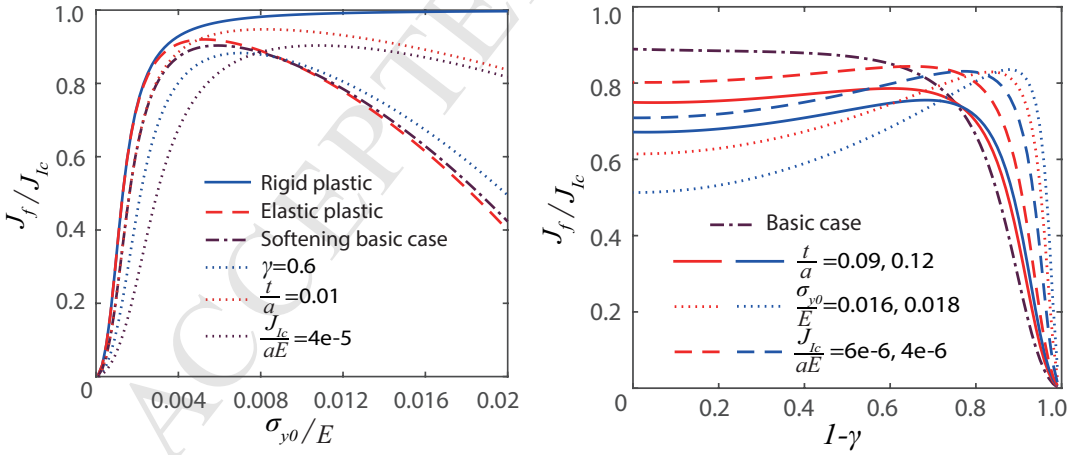

(a) (b)

Fig. 11. Influence of the plastic properties of the strips on the effective fracture toughness of the tensile central notched plate with co-planar heterogeneous strips. (a) The influence of the yield stress of the strips, predicted by Eqns. (14a), (14c), (15c) and

(16c) with $a = 5\text{mm}$, $t = 0.036a$, $E = 100\text{GPa}$, $J_{Ic} = 6\text{kN/m}$ and $\gamma = 0.8$. For the softening case, we also explored the sensitivity of J_f on other parameters, as indicated in the figure. (b) The influence of the strength-softening ratio of the strips, where the basic case is plotted using Eqns. (14a) and (14c) with $a = 5\text{mm}$, $t = 0.036a$, $E = 100\text{GPa}$, $\sigma_{y0} = 800\text{MPa}$ and $J_{Ic} = 6\text{kN/m}$, and the other six cases are calculated by changing one parameter of the basic case as denoted in the figure.

5.3. Local fracture toughness of strips

We now explore the influence of the local fracture toughness J_{Ic} of the strips on the effective fracture toughness of the plate, as shown in Fig. 12. It is seen that the local fracture toughness has a similar impact in the rigid plastic strip model, the elastic-perfectly plastic strip model and the softening elastic-perfectly plastic strip model. With the increasing local toughness, the effective toughness converges to a steady number, which implies the existence of an economic choice of the local fracture toughness for toughening. Meanwhile, a greater softening ratio γ or a smaller thickness t gives rise to a higher effective toughness at the steady state.

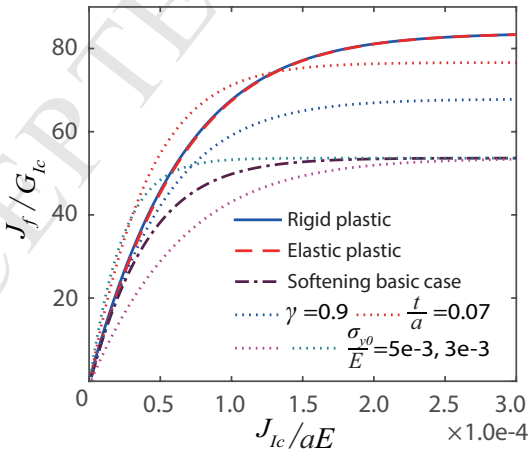

Fig. 12. Influence of the local fracture toughness of the plastic strips on the effective fracture toughness of the tensile central notched plate with co-planar heterogeneous strips, where the rigid plastic, elastic-plastic and softening plastic basic cases are predicted by Eqns. (14a), (14c), (15c) and (16c) with $a = 5\text{mm}$, $t = 0.1a$, $E =$

100GPa, $\sigma_{y0} = 400$MPa and $\gamma = 0.8$, and the other four cases are obtained by changing one parameter of the basic case as denoted.

6. Discussion

Now we compare the theoretical solutions derived from our notch strip-yield model to the results derived from the classic crack strip-yield model (i.e., D-B model). According to Dugdale and Barenblatt's rigid plastic assumption (Dugdale, 1960; Barenblatt, 1962), the uniform normal stress σ_{y0} is applied on the virtual crack surfaces and there is the relationship $G_s = G_{Ic} = 0$. We obtain the following solutions to the plastic strip length s_f', the effective fracture strength σ_f' and the effective fracture strength toughness J_f' for the tensile fractured plate respectively:

$$s_f' = a(\mathrm{e}^{\frac{\pi E J_{Ic}}{8a\sigma_{y0}^2}} - 1), \tag{22a}$$

$$\sigma_f' = \frac{2\sigma_{y0}}{\pi}\mathrm{acos}(e^{-\frac{\pi E J_{Ic}}{8a\sigma_{y0}^2}}), \tag{22b}$$

$$J_f' = \frac{4a\sigma_{y0}^2}{\pi E}\mathrm{acos}^2(e^{-\frac{\pi E J_{Ic}}{8a\sigma_{y0}^2}}). \tag{22c}$$

It is noted that Eqns. (22a), (22b) and (22c) have the same form but different coefficients than Eqns. (16a), (16b) and (16c), respectively. Because the material is supposed to obey the von Mises yield criterion in the present work, a uniform normal loading stress $\frac{2\sigma_{s0}}{\sqrt{3}}$ is assumed on the virtual notch surfaces according to Hill's solution to the necking localization problems (Hill, 1952). Therefore, the two models both with the rigid plasticity assumption predict different results: the D-B model predicts greater yield-strip length, smaller fracture strength and smaller toughness than the presented with the $\frac{2\sigma_{s0}}{\sqrt{3}}$ assumption, as shown in Fig. 13. However, if the Tresca yield criterion is

used, the normal stress on the virtual surfaces should be σ_{y0} (Hill, 1952), i.e., the same as that in the D-B model. According to Hill (1952), the uniform normal stress assumption is reasonable only when the plastic strip length is approximately greater than the notch root radius. It implies that all the predictions with small plastic length are lack of accuracy and should be neglected, including the predictions of the elastic-perfectly plastic model and the softening plastic model, as seen in Fig. 13.

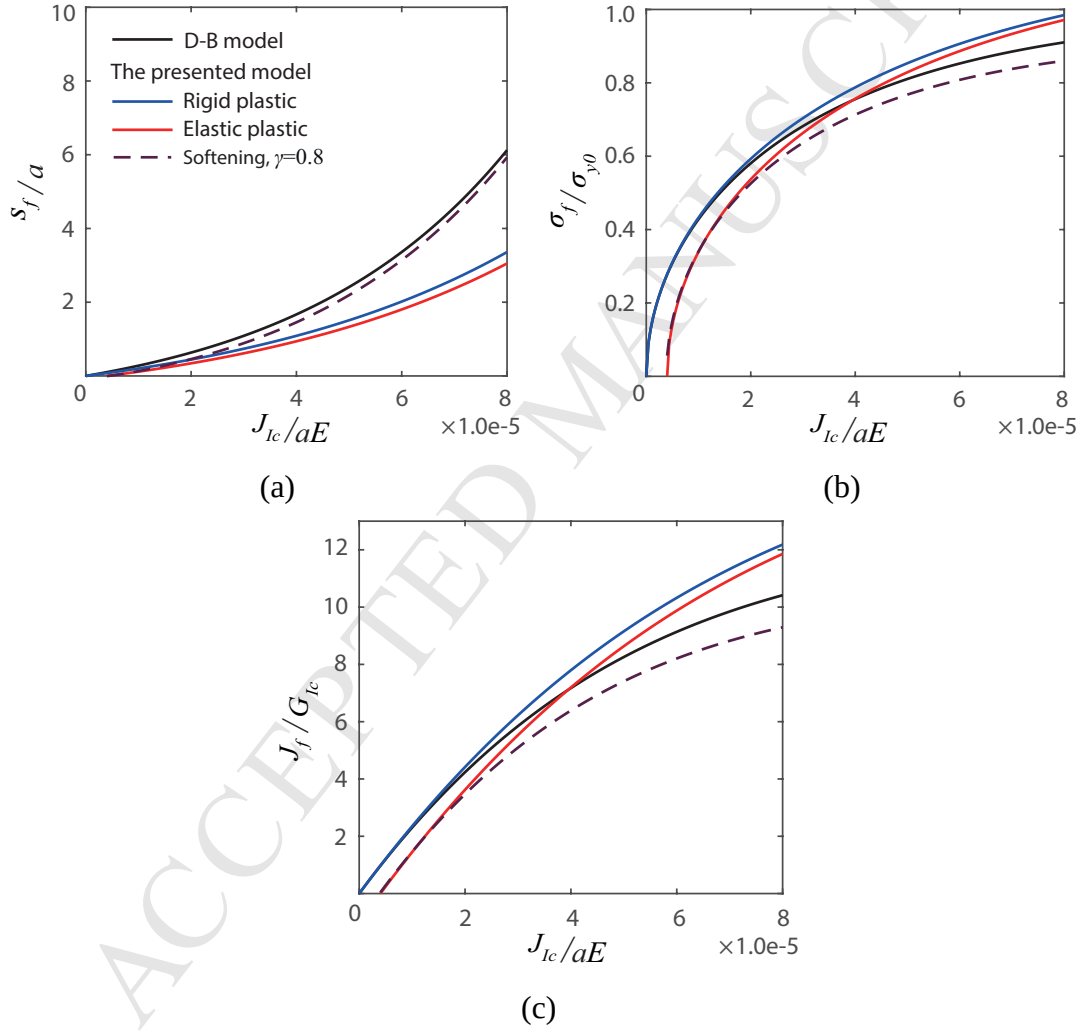

Fig. 13. Comparison of the D-B model (Dugdale, 1960; Barenblatt, 1962) and the present notch yield-strip model, where the following parameters are used: $a = 0.005\text{m}$, $E = 100\text{GPa}$, $\sigma_{y0} = 400\text{MPa}$, $G_{Ic} = 2000\text{N/m}$ and $J_{Ic} = 0\sim40000\text{N/m}$. (a) Normalized length of the co-planar plastic strips in the tensile fractured plate predicted

by Eqns. (22a), (16a), (15a) and (14a). (b) The corresponding normalized fracture strength of the plate predicted by Eqns. (22b), (16b), (15b) and (14b). (c) The corresponding normalized effective fracture toughness predicted by Eqns. (22c), (16c), (15c) and (14c).

Heretofore, we assume the symmetrical branching strips with respect to the crack plane near the notch tips in the plate. In the presence of imperfections, it is common that one kinking plastic strip appears first and then the symmetrical one follows. That is typically seen in BMG specimens with notches subjected to mode I type of loading. However, the strengthening and toughening influence of other strip types having the same material constitutive relationship but different geometry is still worth exploring. As demonstrated in Fig. 14, we have obtained the FE results of two non-branching strip scenarios with one kinking plastic strip around the notch tip, which shed light on the understanding of the strip geometry influence. We see that the one kinking strip increases the effective fracture strength (obviously also the toughness) much greater than the symmetrical branching strips do. In the particular case of fracture strength, we found that when the fitting value m is selected as 5.1 our solution Eqn. (21a) captures well with the dependence of fracture strength on branching angle. It seems to imply that the strips with different geometry may only result in a different value of the fitting parameter m in Eqn. (21). Therefore, our conclusions about the strengthening and toughening influence of the yield-strip ought to be qualitatively the same for different strip geometries.

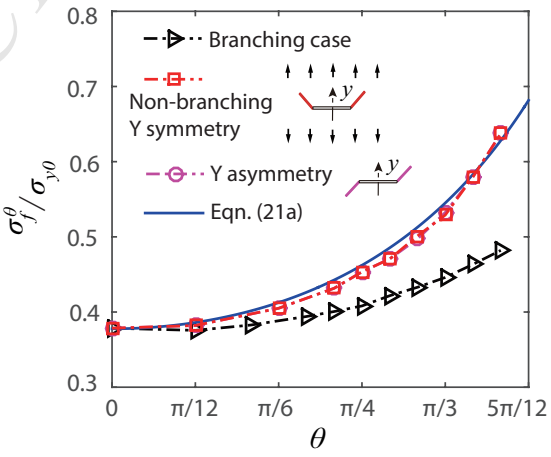

Fig. 14. Comparison of the effective fracture strength for the branching and non-branching plastic strip scenarios using FE simulations. The following parameters are used: $a = 5\text{mm}$, $t = 0.036a$, $E = 100\text{GPa}$, $E_s = E/2$, $\sigma_{y0} = 400\text{MPa}$ and $\gamma = 0.8$. The exponent m in Eqn. (21a) is 5.1.

7. Conclusions

In this work, we investigate the influence of heterogeneous strips on the effective fracture strength and toughness of the central notched plate via theoretical analysis and FE calculation based on a notch strip-yield model modified from the crack strip-yield model (Barenblatt, 1962; Dugdale, 1960). We demonstrate how the strips' branching angle, thickness, yield stress, flow stress, softening modulus and fracture toughness affect the macroscopic fracture strength or fracture toughness in such a plate. We find that the effective fracture toughness of the plate mainly depends on five dimensionless quantities: the strips' branching angle θ, dimensionless thickness $\frac{t}{a}$, yield stress $\frac{\sigma_{y0}}{E}$, local fracture toughness $\frac{J_{Ic}}{aE}$ and strength-softening ratio γ. The influence factors of the heterogeneous strips on the toughening behavior are revealed analytically, and the following conclusions are drawn:

(1) Branching brittle interfaces toughen the plate, and the effective fracture toughness of the plate are proportional to $\left(\sec\frac{\theta}{2}\right)^4$. The branching angle of the plastic strips increases the effective fracture toughness of the plate and is proportional to $\left(\sec\frac{\theta}{2}\right)^{2.6}$, while the effective fracture toughness may either increase or decrease when the strip thickness increases. The exact trend is sensitive to the strength-softening ratio, dimensionless yield stress and local toughness of the strips.

(2) Within a certain range of the yield stress and softening ratio, the plastic strips maximize the effective fracture toughness of the plate. Our results on the toughening influence of plastic strips address some fundamental aspects about the macro fracture

toughness of the local heterogeneous solid. They present a theoretical guide for the design of both strong and tough materials with localized plastic strips.

Acknowledgments

The authors acknowledge the supports from the National Natural Science Foundation of China (NSFC) (Grant No. 11425211, 11790291) and the Strategic Priority Research Program of the Chinese Academy of Sciences (XDB22020200), as well as the support from the Foshan University (Contact No. gg07084).

References

Anand, L., Aslan, O., Chester, S.A., 2012. A large-deformation gradient theory for elastic–plastic materials: Strain softening and regularization of shear bands. International Journal of Plasticity 30-31, 116-143.

Anderson, T.L., 2005. Fracture mechanics: Fundamentals and Applications. CRC Press, Boca Raton, Florida, pp. 18-84.

Argon, A.S., Cohen, R.E., 1990. Crazing and toughness of block copolymers and blends, Crazing in Polymers Vol. 2. Springer Berlin Heidelberg, Berlin, Heidelberg, pp. 301-351.

Argon, A.S., Hannoosh, J.G., 1977. Initiation of crazes in polystyrene. Philosophical Magazine 36, 1195-1216.

Barenblatt, G.I., 1962. The mathematical theory of equilibrium cracks in brittle fracture. Advances in Applied Mechanics 7, 55-129.

Barthelat, F., 2014. Designing nacre-like materials for simultaneous stiffness, strength and toughness: Optimum materials, composition, microstructure and size. Journal of the Mechanics and Physics of Solids 73, 22-37.

Barthelat, F., 2007. Biomimetics for next generation materials. Philosophical Transactions of the Royal Society A 365, 2907-2919.

Barthelat, F., Espinosa, H.D., 2007. An experimental investigation of deformation and fracture of nacre-mother of pearl. Experimental Mechanics 47, 311-324.

Becher, P.F., Hsueh, C., Angelini, P., Tiegs, T.N., 1988. Toughening behavior in whisker-reinforced ceramic matrix composites. Journal of the American Ceramic Society 71, 1050-1061.

Bilby, B., Cottrell, A., Swinden, K., 1963. The spread of plastic yield from a notch. Proceedings of the Royal Society of London A: Mathematical, Physical and Engineering Sciences. The Royal Society, pp. 304-314.

Bohnert, C., Schmitt, N.J., Weygand, S.M., Kraft, O., Schwaiger, R., 2016. Fracture toughness characterization of single-crystalline tungsten using notched micro-cantilever specimens. International Journal of Plasticity 81, 1-17.

Budiansky, B., Hutchinson, J.W., 1978. Analysis of closure in fatigue crack growth. Journal of Applied Mechanics 45, 267-276.

Burdekin, F.M., Stone, D.E.W., 1966. The crack opening displacement approach to fracture mechanics in yielding materials. Journal of Strain Analysis for Engineering Design 1, 145-153.

Chandler, M.R., Meredith, P.G., Brantut, N., Crawford, B.R., 2016. Fracture toughness anisotropy in shale. Journal of Geophysical Research: Solid Earth 121, 1706-1729.

Chen, Y., Dai, L.H., 2016. Nature of crack-tip plastic zone in metallic glasses. International Journal of Plasticity 77, 54-74.

Das, J., Tang, M.B., Kim, K.B., Theissmann, R., Baier, F., Wang, W.H., Eckert, J., 2005. “Work-hardenable” ductile bulk metallic glass. Physical Review Letters 94, 205501.

Demetriou, M.D., Launey, M., Garrett, G., Schramm, J.P., Hofmann, D.C., Johnson, W.L., Ritchie, R.O., 2011. A damage-tolerant glass. Nature Materials 10, 123-128.

Dowling, A.R., Townley, C.H.A., 1975. Effect of defects on structural failure: A two-criteria approach. International Journal of Pressure Vessels and Piping 3, 77-107.

Dugdale, D.S., 1960. Yielding of steel sheets containing slits. Journal of the Mechanics and Physics of Solids 8, 100-104.

Erdogan, F., 2000. Fracture mechanics. International Journal of Solids and Structures 37, 171-183.

Estevez, R., Tijssens, M.G.A., Der Giessen, E.V., 2000. Modeling of the competition between shear yielding and crazing in glassy polymers. Journal of the Mechanics and Physics of Solids 48, 2585-2617.

Friedrich, K., 1983. Crazes and shear bands in semi-crystalline thermoplastics. Crazing in Polymers, 225-274.

Galeski, A., 2003. Strength and toughness of crystalline polymer systems. Progress in Polymer Science 28, 1643-1699.

Gao, H., Zhang, T., Tong, P., 1997. Local and global energy release rates for an electrically yielded crack in a piezoelectric ceramic. Journal of the Mechanics and Physics of Solids 45, 491-510.

Gdoutos, E.E., 2005. Fracture Mechanics. Springer Netherlands, Dordrecht, The Netherlands, pp. 67.

Gupta, H.S., Wagermaier, W., Zickler, G.A., Aroush, D.R., Funari, S.S., Roschger, P., Wagner, H.D., Fratzl, P., 2005. Nanoscale deformation mechanisms in bone. Nano Letters 5, 2108-2111.

He, Q., Shang, J.K., Ma, E., Xu, J., 2012. Crack-resistance curve of a Zr-Ti-Cu-Al bulk metallic glass with extraordinary fracture toughness. Acta Materialia 60, 4940-4949.

Hillerborg, A., 1991. Application of the fictitious crack model to different types of materials. International Journal of Fracture 51, 95-102.

Hofmann, D.C., Suh, J., Wiest, A., Duan, G., Lind, M., Demetriou, M.D., Johnson, W.L., 2008. Designing metallic glass matrix composites with high toughness and tensile ductility. Nature 451, 1085-1089.

Hossain, M.Z., Hsueh, C.J., Bourdin, B., Bhattacharya, K., 2014. Effective toughness of heterogeneous media. Journal of the Mechanics and Physics of Solids 71, 15-32.

Hussain, M., Pu, S., Underwood, J., 1973. Strain energy release rate for a crack under combined mode I and mode II. Proceedings of the 1973 National Symposium on Fracture Mechanics. ASTM Special Technical Publication 560, pp. 2-28.

Hutchinson, J.W., 1968. Plastic stress and strain fields at a crack tip. Journal of the Mechanics and Physics of Solids 16, 337-342.

Hutchinson, J.W., Suo, Z., 1992. Mixed mode cracking in layered materials. Advances in Applied Mechanics 29, 63-191.

Irwin, G., 1957. Analysis of stresses and strains near the end of a crack traversing a plate. Journal of Applied Mechanics 24, 361–364.

Hill, R., 1952. On discontinuous plastic states, with special reference to localized necking in thin sheets. Journal of the Mechanics and Physics of Solids 1, 19-30.

Keten, S., Xu, Z., Ihle, B., Buehler, M.J., 2010. Nanoconfinement controls stiffness, strength and mechanical toughness of B-sheet crystals in silk. Nature Materials 9, 359-367.

Kinloch, A.J., Shaw, S.J., Tod, D.A., Hunston, D.L., 1983. Deformation and fracture behaviour of a rubber-toughened epoxy: 1. Microstructure and fracture studies. Polymer 24, 1341-1354.

Lee, L., Mandell, J., McGarry, F., 1987. Fracture toughness and crack instability in tough polymers under plane strain conditions. Polymer Engineering & Science 27, 1128-1136.

Lei, X., Li, C., Shi, X., Xu, X., Wei, Y., 2015. Notch strengthening or weakening governed by transition of shear failure to normal mode fracture. Sci Rep 5, 10537.

Lewandowski, J.J., Shazly, M., Nouri, A.S., 2006. Intrinsic and extrinsic toughening of metallic glasses. Scripta Materialia 54, 337-341.

Liu, Y.H., Wang, G., Wang, R.J., Pan, M.X., Wang, W.H., 2007. Super plastic bulk metallic glasses at room temperature. Science 315, 1385-1388.

Lowhaphandu, P., Lewandowski, J.J., 1998. Fracture toughness and notched toughness of bulk amorphous alloy: Zr-Ti-Ni-Cu-Be. Scripta Materialia 38, 1811-1817.

McAuliffe, C., Waisman, H., 2015. On the importance of nonlinear elastic effects in shear band modeling. International Journal of Plasticity 71, 10-31.

Newman, J.C., 1984. A crack opening stress equation for fatigue crack growth. International Journal of Fracture 24, R131-R135.

Nguyen, N.H.T., Bui, H.H., Nguyen, G.D., Kodikara, J., 2017. A cohesive damage-plasticity model for DEM and its application for numerical investigation of soft rock fracture properties. International Journal of Plasticity 98, 175-196.

Jiang, M.Q., Wang, W.H., Dai, L.H., 2009. Prediction of shear-band thickness in metallic glasses. Scripta Materialia 60, 1004-1007.

Jiang, W.H., Atzmon, M., 2006. Mechanically-assisted nanocrystallization and defects in amorphous alloys: A high-resolution transmission electron microscopy study. Scripta Materialia 54, 333-336.

Li, J., Spaepen, F., Hufnagel, T.C., 2002. Nanometre-scale defects in shear bands in a metallic glass. Philosophical Magazine A 82, 2623-2630.

Munch, E., Launey, M.E., Alsem, D.H., Saiz, E., Tomsia, A.P., Ritchie, R.O., 2008. Tough, bio-inspired hybrid materials. Science 322, 1516-1520.

Na, S., Sun, W., Ingraham, M.D., Yoon, H., 2017. Effects of spatial heterogeneity and material anisotropy on the fracture pattern and macroscopic effective toughness of Mancos Shale in Brazilian tests. Journal of Geophysical Research: Solid Earth 122, 6202-6230.

Naglieri, V., Gludovatz, B., Tomsia, A.P., Ritchie, R.O., 2015. Developing strength and toughness in bio-inspired silicon carbide hybrid materials containing a compliant phase. Acta Materialia 98, 141-151.

Narisawa, I., 1987. Fracture and toughness of crystalline polymer solids. Polymer Engineering & Science 27, 41-45.

Niebel, T.P., Bouville, F., Kokkinis, D., Studart, A.R., 2016. Role of the polymer phase in the mechanics of nacre-like composites. Journal of the Mechanics and Physics of Solids 96, 133-146.

Nuismer, R., 1975. An energy release rate criterion for mixed mode fracture. International Journal of Fracture 11, 245-250.

Olf, H.G., Peterlin, A., 1974. Crazing and fracture in crystalline, isotactic polypropylene and the effect of morphology, gaseous environments, and temperature. Journal of Polymer Science Part B 12, 2209-2251.

Pardoen, T., Ferracin, T., Landis, C.M., Delannay, F., 2005. Constraint effects in adhesive joint fracture. Journal of the Mechanics and Physics of Solids 53, 1951-1983.

Parrinello, F., Failla, B., Borino, G., 2009. Cohesive–frictional interface constitutive model. International Journal of Solids and Structures 46, 2680-2692.

Podsiadlo, P., Kaushik, A.K., Arruda, E.M., Waas, A.M., Shim, B.S., Xu, J., Nandivada, H., Pumplin, B.G., Lahann, J., Ramamoorthy, A., 2007. Ultrastrong and stiff layered polymer nanocomposites. Science 318, 80-83.

Qiao, J., Jia, H., Liaw, P.K., 2016. Metallic glass matrix composites. Materials Science and Engineering: Reports 100, 1-69.

Rice, J.R., 1968. A path independent integral and the approximate analysis of strain concentration by notches and cracks. Journal of Applied Mechanics 35, 379-386.

Rice, J.R., Rosengren, G.F., 1968. Plane strain deformation near a crack tip in a power-law hardening material. Journal of the Mechanics and Physics of Solids 16, 1-12.

Rice, J.R., Sorensen, E.P., 1978. Continuing crack-tip deformation and fracture for plane-strain crack growth in elastic-plastic solids. Journal of the Mechanics and Physics of Solids 26, 163-186.

Schroers, J., Johnson, W.L., 2004. Ductile bulk metallic glass. Physical Review Letters 93, 255506-255700.

Shao, Y., Zhao, H.P., Feng, X.Q., Gao, H., 2012. Discontinuous crack-bridging model for fracture toughness analysis of nacre. Journal of the Mechanics and Physics of Solids 60, 1400-1419.

Shih, C.F., 1981. Relationships between the J-integral and the crack opening displacement for stationary and extending cracks. Journal of the Mechanics and Physics of Solids 29, 305-326.

Simulia, D., 2011. ABAQUS 6.11 Analysis User's Manual. Dassault Systems, Simulia Corporation.

Spurr, O.K., Niegisch, W.D., 1962. Stress crazing of some amorphous thermoplastics. Journal of Applied Polymer Science 6, 585-599.

Sun, B.A., Wang, W.H., 2015. The fracture of bulk metallic glasses. Progress in Materials Science 74, 211-307.

Su, C., Wei, Y.J., Anand, L., 2004. An elastic-plastic interface constitutive model: application to adhesive joints. International Journal of Plasticity 20, 2063-2081.

Tada, H., Paris, P., Irwin, G., 2000. The analysis of cracks handbook. ASME Press, New York, pp. 143.

Tang, Z., Kotov, N.A., Magonov, S., Ozturk, B., 2003. Nanostructured artificial nacre. Nature Materials 2, 413-418.

Tvergaard, V., Hutchinson, J.W., 1992. The relation between crack growth resistance and fracture process parameters in elastic-plastic solids. Journal of the Mechanics and Physics of Solids 40, 1377-1397.

Tvergaard, V., Hutchinson, J.W., 1993. The influence of plasticity on mixed mode interface toughness. Journal of the Mechanics and Physics of Solids 41, 1119-1135.

Tvergaard, V., Hutchinson, J.W., 1996. On the toughness of ductile adhesive joints. Journal of the Mechanics and Physics of Solids 44, 789-800.

Wei, Y., 2014. A stochastic description on the traction-separation law of an interface with non-covalent bonding. Journal of the Mechanics and Physics of Solids 70, 227-241.

Wei, Y., Gao, H., Bower, A.F., 2009. Numerical simulations of crack deflection at a twist-misoriented grain boundary between two ideally brittle crystals. Journal of the Mechanics and Physics of Solids 57, 1865-1879.

Wei, Y., Hutchinson, J.W., 1997. Steady-state crack growth and work of fracture for solids characterized by strain gradient plasticity. Journal of the Mechanics and Physics of Solids 45, 1253-1273.

Yamada, Y., Ziegler, B., Jr, J.C.N., 2011. Application of a strip-yield model to predict crack growth under variable-amplitude and spectrum loading – Part 1: Compact specimens. Engineering Fracture Mechanics 78, 2597-2608.

Zeng, X., Wei, Y., 2017. Crack deflection in brittle media with heterogeneous interfaces and its application in shale fracking. Journal of the Mechanics and Physics of Solids 101, 235-249.

Zhou, X., Chen, C., 2016. Strengthening and toughening mechanisms of amorphous/amorphous nanolaminates. International Journal of Plasticity 80, 75-85.

Highlights

1) A notch strip-yield model accounting for strain softening effect is presented;

2) Analytical solutions for the effective fracture strength and toughness solution are obtained for particular boundary-value problems;

3) Governing dimensionless quantities on fracture toughness are identified.